Photoinduced Conversion of Silver Nanospheres to Nanoprisms

Rongchao Jin, *et al.*

Science **294**, 1901 (2001);
DOI: 10.1126/science.1066541

scribed: GST-HuR and GST-pp32 (*43*); GST-Trn1, GST-Trn2, and Myc-hnRNP A1 (plasmids encoding these proteins were a gift from S. Nakielny and G. Dreyfuss, University of Pennsylvania, Philadelphia, PA) (*18*–*20*).
68. Polyclonal antibody to Trn2 (αTrn2) was generated as described (*43*) by injecting a rabbit with 500 μg of GST-Trn2. The αTrn2 polyclonal and αTrn1 monoclonal (D45, gift of G. Dreyfuss) (*19*, *20*) antibodies exhibited no detectable cross reactivity by Western blotting of recombinant GST-Trn1 and GST-Trn2 proteins (*57*).
69. I. E. Gallouzi, C. M. Brennan, J. A. Steitz, *RNA* **7**, 1348 (2001).
70. A. Schneider-Gadicke *et al.*, *Cancer Res.* **48**, 2969 (1988).
71. P. A. Lazo, *Eur. J. Biochem.* **165**, 393 (1987).
72. N. S. Levy, S. Chung, H. Furneaux, A. P. Levy, *J. Biol. Chem.* **273**, 6417 (1998).
73. W. Wang *et al.*, *Mol. Cell. Biol.* **20**, 760 (2000).
74. W. van der Houven van Oordt *et al.*, *J. Cell Biol.* **149**, 307 (2000).
75. M. S. Moore, G. Blobel, *Trends Biochem. Sci.* **19**, 211 (1994).
76. S. R. Wente, G. Blobel, *J. Cell Biol.* **123**, 275 (1993).
77. Peptides were synthesized by standard Fmoc chemistry, purified, and analyzed by reverse-phase high-pressure liquid chromatography and mass spectrometry by the W. M. Keck Biotechnology Resource Center at Yale University School of Medicine.
78. Single-letter abbreviations for the amino acid residues are as follows: A, Ala; C, Cys; D, Asp; E, Glu; F, Phe; G, Gly; H, His; I, Ile; K, Lys; L, Leu; M, Met; N, Asn; P, Pro; Q, Gln; R, Arg; S, Ser; T, Thr; V, Val; W, Trp; and Y, Tyr.
79. C. Elfgang *et al.*, *Proc. Natl. Acad. Sci. U.S.A.* **96**, 6229 (1999).
80. HeLa and L929 cells were cultured as described (*43*).
81. To detect c-fos mRNA, HeLa cells were starved in media lacking serum for 48 hours; then 10% fetal bovine serum (GIBCO) was added for 1 hour to stimulate c-fos transcription. Peptides were added 3 hours before serum stimulation and were present until the cells were fixed 1 hour later for in situ hybridization. No signal was obtained when cells were not serum induced (*57*).
82. In situ hybridization was performed with a 3′ digoxigenin-labeled antisense deoxyoligonucleotide probe for *c-fos* mRNA (panels 1 to 8) or for DHFR (dihydrofolate reductase) mRNA (panels 9 to 12) or with oligo(dT)$_{40}$ (panels 13 to 20) to visualize total cellular poly(A)$^+$ RNA. The probes were complementary to nucleotides 288 to 328 [from the translation start site of c-fos (Calbiochem)] or to nucleotides 530 to 569 for DHFR (synthesized by the Keck Facility, Yale University) and were used at 5 ng/ml with a 1:200 dilution of sheep antibody to digoxigenin Fab-rhodamine (Boehringer). Identical results were obtained with probes for the 3′ UTR of *c-fos* (complementary to nucleotides 3363 to 3473; a gift from J.-L. Veyrune) or DHFR (nucleotides 898 to 937; Keck Facility). All mRNA-specific probes gave single bands on Northern blots (*57*).
83. ^{35}S-labeled proteins were produced by in vitro transcription-translation (*19*) of 1 mg of pcDNA3-HuR (*38*), pcDNA Myc-hnRNP A1 (*18*), or pHybLex-HNS [made by subcloning the Eco RI–Xho I fragment of pcDNA3-HuR into the Eco RI–Xho I restriction sites of the pHybLex vector (Invitrogen)] plasmid. Far-Western blotting was performed as described (*20*).
84. For the bottom two panels of Fig. 5A, 10 μg each of GST or the indicated GST fusion protein was incubated for 1 hour at 4°C with 40 μl of glutathione-Sepharose (Pharmacia) in 500 μl of binding buffer [50 mM tris-HCl, 400 mM NaCl, 5 mM MgOAc, leupeptin (2 μg/ml), pepstatin (2 μg/ml), and 0.5% aprotinin (pH 7.5)], also used for washing.
85. We are most grateful to C. Brennan for help in generating the antibody to Trn2 and for valuable discussions and suggestions. We G. G. Carmichael, K. T. Tycowski, L. B. Weinstein, T. S. McConnell, J. Lykke-Andersen, and T. Hirose for comments on the manuscript and many helpful suggestions. We express our gratitude to S. Nakielny and G. Dreyfuss for providing the Trn1, Trn2, and hnRNP A1 plasmids as well as the monoclonal antibody to Trn1 and to S. Pinol Roma for the antibody to hnRNP A1 (4B10). This work was supported by grant CA16038 from the NIH. J.S. is an investigator of the Howard Hughes Medical Institute.

24 July 2001; accepted 12 October 2001

Photoinduced Conversion of Silver Nanospheres to Nanoprisms

Rongchao Jin,[1] YunWei Cao,[1] Chad A. Mirkin,[1]* K. L. Kelly,[1] George C. Schatz,[1]* J. G. Zheng[2]

A photoinduced method for converting large quantities of silver nanospheres into triangular nanoprisms is reported. The photo-process has been characterized by time-dependent ultraviolet-visible spectroscopy and transmission electron microscopy, allowing for the observation of several key intermediates in and characteristics of the conversion process. This light-driven process results in a colloid with distinctive optical properties that directly relate to the nanoprism shape of the particles. Theoretical calculations coupled with experimental observations allow for the assignment of the nanoprism plasmon bands and for the first identification of two distinct quadrupole plasmon resonances for a nanoparticle. Unlike the spherical particles they are derived from that Rayleigh light-scatter in the blue, these nanoprisms exhibit scattering in the red, which could be useful in developing multicolor diagnostic labels on the basis not only of nanoparticle composition and size but also of shape.

Size provides important control over many of the physical and chemical properties of nanoscale materials, including luminescence, conductivity, and catalytic activity (*1*, *2*). Colloid chemists have gained excellent control over particle size for several spherical metal and semiconductor compositions, which has led to the discovery of quantum confinement in colloidal nanocrystals and to the use of such structures as probes for biological diagnostic applications, LED materials, lasers, and Raman spectroscopy–enhancing materials (*3*–*10*). However, the challenge of synthetically controlling particle shape has been met with limited success. Nevertheless, some physical and solid-state chemical deposition methods have been developed for making semiconductor and metal nanowires, nanobelts, and nanodots (*11*–*13*). Now, there are also a variety of methods for making rods with somewhat controllable aspect ratios using seeding approaches (*14*, *15*) and electrochemical (*16*, *17*) and membrane-templated syntheses (*18*). Less is known about bulk solution synthetic methods for nonspherical particles, although methods do exist for making colloidal samples of Pt cubes and pyramids (*19*) and PbSe, CdS, and Ni triangles (*20*–*22*). Trace quantities of Au and Ag nanoprisms have been observed as by-products of methods that predominately produce spheres (*23*, *24*). Promising recent work has resulted in methods for synthesizing $BaCrO_4$, CdSe, and Co nanorods and distributions of arrow-, teardrop-, and tetrapod-shaped CdSe nanocrystals (*25*–*28*).

All of these solution methods are based on thermal processes, and, in most cases with the exception of rods, they yield relatively small quantities of the desired particle shape. Thus, the development of bulk solution synthetic methods that offer shape control is of paramount importance if the full potential of these materials is to be realized. Herein, we report a photoinduced method for synthesizing large quantities of silver nanoprisms in high yield in the form of a colloidal suspension. This photo-mediated route has led to a colloid with distinctive optical properties that directly relate to the shape control.

In a typical experiment, spherical silver particles were prepared by injection of $NaBH_4$ solution (50 mM, 1 ml) to an aqueous solution of $AgNO_3$ (0.1 mM, 100 ml) in the presence of trisodium citrate (0.3 mM). Bis(*p*-sulfonatophenyl) phenylphosphine dihydrate dipotassium salt solution (BSPP) (5 mM, 2 ml) was subsequently added by drop-wise addition to the solution as a particle stabilizing agent. The system is then irradiated with a conventional 40-W fluorescent light (General Electric, Cleveland,

[1]Department of Chemistry and Institute for Nanotechnology, [2]Department of Materials Science and Engineering, Northwestern University, 2145 Sheridan Road, Evanston, IL 60208, USA.

*To whom correspondence should be addressed. E-mail: camirkin@chem.nwu.edu (experimental work) or schatz@chem.nwu.edu (theoretical work).

Ohio). A set of color changes not typical for the preparation of spherical particles was observed during the course of the reaction. Initially, the solution turned yellow, characteristic of the spherical particles, but over 70 hours the solution turned green and then finally blue. We observed a decrease in intensity of the characteristic surface plasmon band in the ultraviolet-visible (UV-Vis) spectroscopy for the spherical particles at λ_{max} = 400 nm with a concomitant growth of three new bands of λ_{max} = 335 (weak), 470 (medium), and 670 nm (strong), respectively (Fig. 1). After 70 hours, the band at 400 nm completely disappeared.

Transmission electron microscopy (TEM), when correlated with the time-dependent spectroscopic observations, shows that the initial spherical silver particles (8.0 ± 1.7 nm) were converted to prismatic structures that appear in two dimensions as triangles (Fig. 2). During the initial stages of growth, both spheres and prisms can be seen (Fig. 2B). The latter exhibit edge lengths between 10 and 60 nm. Both the size and population of the Ag prisms increase with time with a concomitant decrease in the number of spherical particles (Fig. 2C). After 70 hours, nearly all of the initial spheres (>99%) are converted to the prismatic structures [edge length = 100 nm and the standard deviation (σ) = 15%] (Fig. 2D). These data clearly show that the silver nanoprisms evolve from the initial spherical nanoparticles.

To gain insight into the mechanistic basis behind this unusual and remarkably efficient conversion of nanospheres to nanoprisms, we investigated the importance of several reaction conditions, including the silver salt precursor and its concentration, the ligand ratio of BSPP to citrate, and light. The reaction is initiated by light at wavelengths between 350 to 700 nm. The conversion does not take place in the dark (over a 2-month time period) or when irradiated with near-infrared light (>700 nm, 40-W fluorescent tube light source with a cutoff filter). Therefore, the reaction, which results in nanoprisms, can be selectively turned on or off simply by controlling the exposure of the colloid to light of the appropriate wavelength. The rate of the reaction decreases as a function of increasing ratio of BSPP to citrate (range 0.01 to 1); however, nanoprisms form over the entire ligand ratio range. Optimum results were obtained with a 0.3:1 ratio. Comparable results are also obtained with spherical particles formed from $AgClO_4$.

We have identified three distinctive stages in nanoprism formation: induction, growth, and termination (Fig. 1B). Detailed TEM studies revealed that during the induction period extremely small spherical silver clusters (2 to 4 nm) were formed, which were not observed in the solution containing the initial spherical particles. These silver clusters may have formed from either fragmentation or dissolution of the larger particles. Photoinduced fragmentation of silver nanoparticles (visible laser at 532 nm) has been observed by Hartland and co-workers (*29*), albeit with a much higher intensity source. The small nanoprisms (5- to 10-nm edge lengths; Fig. 2B, arrow) observed herein form concurrently with the formation of these small clusters. The silver nanoprisms then act as seeds and grow as the small spherical crystals are digested (Scheme 1). Once the spherical particles and small nanoclusters are consumed, the reaction terminates. The photoinduced conversion of silver particles into small clusters makes the use of light an efficient way to control the growth of the silver nanoprisms. Other researchers have used visible lasers, UV, or γ irradiation to prepare spherical silver nanocrystals from silver salts in the presence of organic reducing agents (*30*, *31*), and, typically, photoinduced reduction mechanisms are invoked to describe such processes. Such mechanisms are different than the growth mechanism proposed herein for the silver nanoprisms in which the spherical silver particles begin in the reduced state and are exclusively transformed into nanoprisms through the light-induced ripening process.

TEM images and electron energy loss spectroscopy analysis (EELS) show that the particles formed in this unusual reaction are indeed silver nanoprisms, not triangular tetrahedra (Fig. 3). The triangular thickness fringes expected for triangular tetrahedra are not observed in the TEM. The EELS data show that each nanoprism has a flat top and bottom (Fig. 3A). Upon evaporation of solvent, the silver nanoprisms assemble into "stacks" on the TEM grids (Fig. 3B), which allow precise measure-

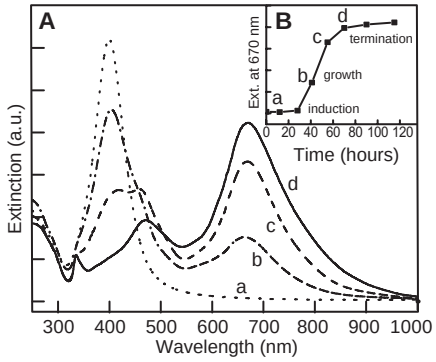

Fig. 1. (**A**) Time-dependent UV-Vis spectra showing the conversion of silver nanospheres to nanoprisms (a) before irradiation and after (b) 40, (c) 55, and (d) 70 hours of irradiation. (**B**) Corresponding extinction profiles at 670 nm as a function of time.

Scheme 1.

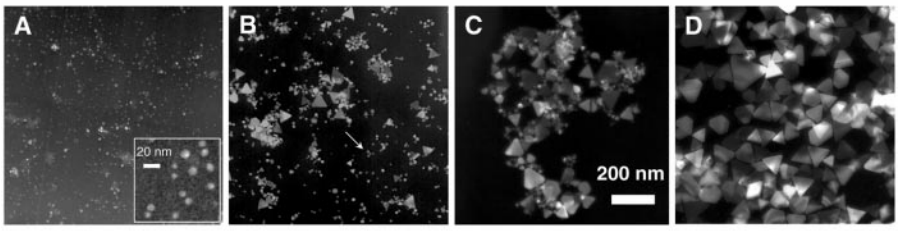

Fig. 2. TEM images (reverse print) mapping the morphology changes (**A**) before irradiation and after (**B**) 40, (**C**) 55, and (**D**) 70 hours of irradiation. Except for the inset in (A), the scale bar is 200 nm for all four images.

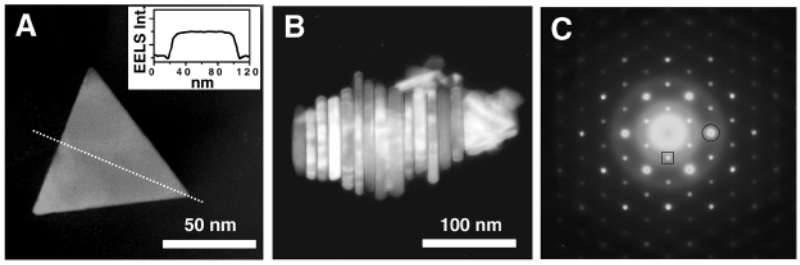

Fig. 3. (**A**) EELS mapping analysis showing the flat-top morphology of the Ag nanoprisms. Inset shows the EELS intensity over the line scan (dotted line through triangle axis). (**B**) Stacks of Ag nanoprisms assembled in a top-to-base manner on a carbon film–coated Cu grid. (**C**) Electron diffraction analysis of individual Ag nanoprisms. The spot array, diagnostic of a hexagonal structure, is from the [111] orientation of an individual Ag nanoprism lying flat on the substrate with its top perpendicular to the electron beam. On the basis of three-zone axis analysis (not shown), the crystal structure of the Ag nanoprism was determined to be an fcc structure. The intense spots in the [111] zone axis are allowed {220} Bragg reflections (e.g., circled spot, corresponding to the lattice spacing of 1.44 Å), and the sharp weak spot in the center of the triangles formed by the strong spots is indexed as $\frac{1}{3}\{\bar{4}22\}$ (e.g., boxed spot, corresponding to the lattice spacing of 2.50 Å).

ment of their thickness (15.6 ± 1.4 nm). These stacks appear as nanorods in the two-dimensional TEM images, but tilting experiments confirm that they are nanoprisms. Each nanoprism is a single crystal with a lattice spacing of 1.44 Å, as shown by electron diffraction analysis (Fig. 3C). Detailed TEM investigations (tilting diffraction with three zone axes) of individual silver nanoprisms have shown that the 1.44 Å lattice spacing corresponds to Bragg diffraction from their {220} lattice planes [face-centered cubic (fcc)]. Therefore, the top crystal face of each nanoprism must be (111). An additional set of relatively weak spots in the diffraction pattern, corresponding to $\frac{1}{3}\{\bar{4}22\}$ with a 2.5 Å spacing (*23*), is also observed. These weak diffraction spots derive from the local hexagonal-like structure observable only for a silver (or gold) sample that is atomically flat (*32*, *33*). Taken together, these data are consistent with the structural characterization of these previously unknown particles as thin nanoprisms with atomically flat tops and bottoms.

The large structural anisotropy of these triangular nanoprisms should substantially influence their optical properties, including light-absorption, -scattering, and surface-enhanced Raman spectroscopy (SERS). According to Mie theory (*34*), small spherical nanocrystals—either Ag or Au—should exhibit a single surface plasmon band, whereas anisotropic particles should exhibit two or three bands, depending on their shape. Larger particles can exhibit additional bands, corresponding to quadrupole and higher multipole plasmon excitation. To characterize the extinction spectrum in Fig. 1A(d), we have solved Maxwell's equations for light interacting with a triangular prism using a finite element–based method known as the discrete dipole approximation (DDA) (*35*). The shape and dimensions of the nanoprism (depicted in Fig. 4A) are average representations of the triangular prisms observed in the TEM images (Fig. 2D). Three bands were observed that qualitatively match the wavelengths of the measured spectra [compare Fig. 1A(d) and Fig. 4A]. Examination of the induced polarizations associated with these peaks indicates that the 770-nm peak is the in-plane dipole plasmon resonance, the 470-nm peak is the in-plane quadrupole resonance, and the 340-nm peak is the out-of-plane quadrupole resonance. The out-of-plane dipole resonance at 410 nm is sufficiently weak and broad that it is barely discernable as a shoulder on the 470-nm peak. Additional calculations indicate that the peak at 770 nm is very sensitive to the sharpness of the tips on the triangles. For example, if a 12-nm region at each tip of a prism is removed, the long-wavelength resonance at 770 nm for the perfect prism shifts to 670 nm without changing the other resonances (Fig. 4B). Note that TEM shows that about 20% of the nanoprisms are truncated (Fig. 2D). Therefore, these calculations not only allow us to identify the important features in the spectrum of the nanoprisms but also the subtle relation between particle shape and the frequency of the bands that make up their spectra.

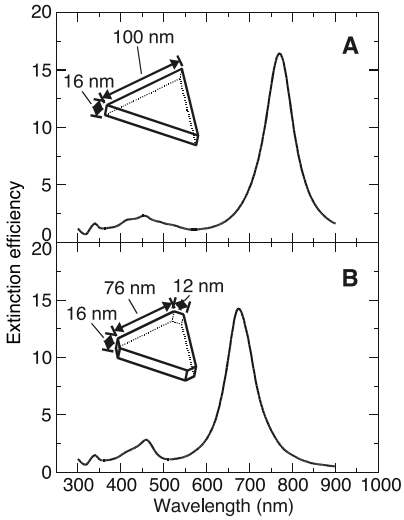

Fig. 4. DDA simulations of the orientation averaged extinction efficiency spectra of two Ag nanoprisms in water. (**A**) A perfectly triangular nanoprism (8512 dipoles are used in the calculation) and (**B**) a truncated triangular nanoprism (7920 dipoles are used for the calculation). Dielectric constant data are taken from (*38*).

These novel nanostructures are unusual and their optical properties are striking. For example, they have provided the first observation of two distinct quadrupole plasmon resonances for a nanoparticle. Unlike the spherical particles from which they are derived that scatter in the blue, they exhibit Rayleigh scattering in the red (Fig. 5A). Light-scattering of metal nanoparticle probes already has been exploited in the development of many biodiagnostic applications (*36*, *37*). Although conventional spherical particles made of gold or silver do not scatter in the red, their scattering properties can be tailored by adjusting their size and composition (Fig. 5, B through E). Therefore, the discovery of these previously unknown nanoprisms and their unusual optical properties points to a way of developing multicolor labels on the basis of nanoparticle shape in addition to composition and size. Lastly, the light-scattering properties of these materials are simply one consequence of controlling particle shape. Indeed, theoretical calculations have predicted that silver nanoprisms should have enormous SERS enhancement factors and second harmonic generation capabilities (*10*, *35*).

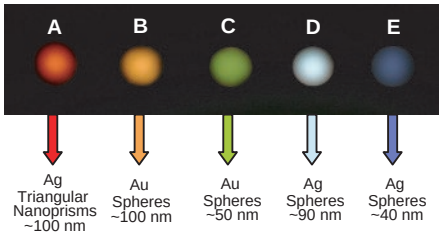

Fig. 5. Rayleigh light-scattering of particles deposited on a microscope glass slide. The slide is used as a planar waveguide, which is illuminated with a tungsten source. The image was taken with a digital camera.

References and Notes

1. A. P. Alivisatos, *Science* **271**, 933 (1996).
2. C. M. Lieber, *Solid State Commun.* **107**, 607 (1998).
3. R. Elghanian, J. J. Storhoff, R. C. Mucic, R. L. Letsinger, C. A. Mirkin, *Science* **277**, 1078 (1997).
4. T. A. Taton, C. A. Mirkin, R. L. Letsinger, *Science* **289**, 1757 (2000).
5. Y. W. Cao, R. Jin, C. A. Mirkin, *J. Am. Chem. Soc.* **123**, 7961 (2001).
6. W. C. W. Chan, S. M. Nie, *Science* **281**, 2016 (1998).
7. Y. Cui, Q. Wei, H. Park, C. M. Lieber, *Science* **293**, 1289 (2001).
8. V. L. Colvin, M. C. Schlamp, A. P. Alivisatos, *Nature* **370**, 354 (1994).
9. V. I. Klimov *et al.*, *Science* **290**, 314 (2000).
10. G. C. Schatz, R. P. Van Duyne, in *Handbook of Vibrational Spectroscopy*, J. M. Chalmers, P. R. Griffiths, Eds. (Wiley, New York, 2002), vol. 1, pp. 759–774.
11. J. T. Hu, T. W. Odom, C. M. Lieber, *Acc. Chem. Res.* **32**, 435 (1999).
12. Z. W. Pan, Z. R. Dai, Z. L. Wang, *Science* **291**, 1947 (2001).
13. C. L. Haynes, R. P. Van Duyne, *J. Phys. Chem. B* **105**, 5599 (2001).
14. N. R. Jana, L. Gearheart, C. J. Murphy, *Chem. Comm.* (2001), p. 617.
15. N. R. Jana, L. Gearheart, C. J. Murphy, *J. Phys. Chem. B* **105**, 4065 (2001).
16. Y. Y. Yu, S. S. Chang, C. L. Lee, C. R. C. Wang, *J. Phys. Chem. B* **101**, 6661 (1997).
17. B. Nikoobakht, Z. L. Wang, M. A. El-Sayed, *J. Phys. Chem. B* **104**, 8635 (2000).
18. C. A. Foss, G. L. Hornyak, J. A. Stockert, C. R. Martin, *J. Phys. Chem.* **98**, 2963 (1994).
19. T. S. Ahmadi, Z. L. Wang, T. C. Green, A. Henglein, M. A. El-Sayed, *Science* **272**, 1924 (1996).
20. J. H. Fendler, F. C. Meldrum, *Adv. Mater.* **7**, 607 (1995).
21. N. Pinna, K. Weiss, J. Urban, M.-P. Pileni, *Adv. Mater.* **13**, 261 (2001).
22. J. S. Bradley, B. Tesche, W. Busser, M. Maase, M. T. Reetz, *J. Am. Chem. Soc.* **122**, 4631 (2000).
23. A. I. Kirkland *et al.*, *Proc. R. Soc. London A* **440**, 589 (1993).
24. T. Klasu, R. Joerger, E. Olsson, C.-G. Granqvist, *Proc. Natl. Acad. Sci. U.S.A.* **96**, 13611 (1999).
25. M. Li, H. Schnablegger, S. Mann, *Nature* **402**, 393 (1999).
26. X. Peng *et al.*, *Nature* **404**, 59 (2000).
27. V. F. Puntes, K. M. Krishnan, A. P. Alivisatos, *Science* **291**, 2115 (2001).
28. L. Manna, E. C. Scher, A. P. Alivisatos, *J. Am. Chem. Soc.* **122**, 12700 (2000).
29. P. V. Kamat, M. Flumiani, G. V. Hartland, *J. Phys. Chem. B* **102**, 3123 (1998).
30. A. Henglein, *Langmuir* **17**, 2329 (2001).
31. M. Prochazka, P. Mojzes, J. Stepanek, B. Vlcková, P.-Y Turpin, *Anal. Chem.* **69**, 5103 (1997).
32. D. Cherns, *Philos. Mag.* **30**, 549 (1974).
33. A. I. Kirkland, D. A. Jefferson, D. G. Duff, P. P. Edwards, *Inst. Phys. Conf. Ser.* **98**, 375 (1990).
34. G. Mie, *Ann. Phys.* **25**, 377 (1908).
35. W. H. Yang, G. C. Schatz, R. P. Van Duyne, *J. Chem. Phys.* **103**, 869 (1995).
36. S. Schultz, D. R. Smith, J. J. Mock, D. A. Schultz, *Proc. Natl. Acad. Sci. U.S.A.* **97**, 996 (2000).
37. T. A. Taton, L. Gang, C. A. Mirkin, *J. Am. Chem. Soc.* **123**, 5164 (2001).
38. E. D. Palik, *Handbook of Optical Constants of Solids* (Academic Press, New York, 1985), pp. 350–357.

39. C.A.M. and G.C.S thank the NSF (CHE-9871903), Army Research Office (DAAG55-97-1-0133), and Air Force Office of Scientific Research (DURINT) for support of this work. S. Li and L. Marks (Northwestern University) are acknowledged for their assistance in the TEM EELS and the TEM diffraction analyses.

25 September 2001; accepted 29 October 2001